Influence of orientation on the evolution of small perturbations in compressible shear layers with inflection points

Mona Karimi[1,*] and Sharath S. Girimaji[1,2]
[1]*Aerospace Engineering Department, Texas A&M University, College Station, Texas 77843, USA*
[2]*Ocean Engineering Department, Texas A&M University, College Station, Texas 77843, USA*
(Received 30 September 2016; published 24 March 2017)

We investigate the influence of orientation on the evolution of small perturbations in compressible shear layers with inflection points. By using linear analysis, we demonstrate that perturbations along the shear plane are most affected by compressibility. The influence of compressibility gradually diminishes with increasing obliqueness of the perturbations with respect to the shear plane. It is demonstrated that the effective gradient Mach number is an appropriate compressibility parameter. We establish that spanwise perturbations, orthogonal to the shear plane, are impervious to compressibility effects. Direct numerical simulations of compressible mixing layers subject to the perturbations at various obliqueness angles verify the analytical findings.

DOI: 10.1103/PhysRevE.95.033112

I. INTRODUCTION

The Rayleigh inflection point criterion is one the hallmarks of incompressible shear layer instability [1]. The Kelvin–Helmholtz instability (KHI) is the principal cause of small perturbation growth and transition to turbulence in general low-speed shear layers with the inflection point. Chandrasekhar was among the first investigators to study the effect of compressibility on KHI [2]. The connection between mixing inhibition in compressible shear layers and KHI suppression has been established in various astrophysical phenomena involving sheared plasma flow [3–5]. The stabilizing effect of compressibility in high-speed turbulent mixing layers is known from numerous experimental investigations [6–9] and numerical simulations [10–13]. Numerical and experimental data indicate a steady decline in mixing layer thickness as the Mach number increases.

In recent work, Karimi and Girimaji [14] formulated a linear initial value problem to investigate the compressibility effect on early behavior of KHI in planar shear flows with a velocity field inflection point. The authors establish that the main physical distinction between high-speed and low-speed mixing layers lies in the flow surrounding the inflection point. In high-speed flows, the inflection-point region is dominated by wave-like dilatational motion due to the action of pressure. The wave-like motion shakes, rather than stirs, the fluid in the inflection-point region. The reversible shaking action inhibits mixing. On the other hand, the inflection-point region in incompressible mixing layers features a vorticity-dominated roll-up motion which leads to entrainment, the onset of instability, and ultimately mixing.

While many of the mixing layer instability studies focus on streamwise perturbations, some studies indicate that the perturbations oblique to the shear plane are also important [15,16]. The degree of perturbation obliqueness plays a critical role in the growth of the perturbation kinetic energy [10,17]. Employing direct numerical simulation (DNS) of the temporally evolving compressible mixing layer, it has been demonstrated that oblique disturbances are more unstable than planar or streamwise disturbances [10]. There is a pronounced difference of structure as the obliqueness angle of the initial perturbation varies in a compressible mixing layer. To elucidate understanding of the effect of compressibility on free shear-layer stability, the influence of perturbation obliqueness on the early growth of instability is investigated.

The objectives of the present work are (i) to perform a linear analysis to establish the influence of perturbation obliqueness on shear layer evolution and (ii) to employ direct numerical simulation (DNS) of full equations to verify the outcomes of the linear analysis. The focus is on the changing character of perturbation pressure field, velocity field, and pressure-velocity interactions as a function of Mach number and obliqueness angle.

The outline of the paper is as follows: The governing equations and linear analysis are presented in Sec. II. Numerical approach including simulation parameters, the initial conditions and boundary conditions is presented in Sec. III. The influence of obliqueness on early time evolution of a compressible mixing layers are investigated in detail in Sec. IV. We conclude with a brief summary of findings in Sec. V.

II. GOVERNING EQUATIONS AND LINEAR ANALYSIS

The three-dimensional, unsteady, compressible Navier–Stokes equations form the basis of analysis and simulation of this study. The conservation equations of mass, momentum, and energy are as follows:

$$\frac{\partial \rho}{\partial t} + \frac{\partial}{\partial x_j}(\rho u_j) = 0, \quad (1)$$

$$\frac{\partial}{\partial t}(\rho u_j) + \frac{\partial}{\partial x_k}(\rho u_j u_k) = -\frac{\partial (p\delta_{jk})}{\partial x_k} + \frac{1}{\mathrm{Re}_l}\frac{\partial \sigma_{jk}}{\partial x_k}, \quad (2)$$

$$\frac{\partial p}{\partial t} + u_j\frac{\partial p}{\partial x_j} = -\gamma p\frac{\partial u_k}{\partial x_k} + \frac{\gamma(\gamma-1)}{\mathrm{Re}_l}\frac{\partial(\sigma_{jk}u_k)}{\partial x_j} + \frac{\gamma}{\mathrm{PrRe}}\nabla^2\left(\frac{p}{\rho}\right), \quad (3)$$

where x_i are the Cartesian coordinates, u_i are the velocity components for $i = 1$–3, ρ is density, and time is denoted by t. The specific-heat ratio is $\gamma = c_p/c_v$. The coefficient of the dynamic viscosity (μ) is assumed to follow Sutherland's law, and λ is the second viscosity coefficient. The thermodynamic

*monak16mpi@gmail.com

pressure p is given by the ideal-gas law: $p = \rho RT$. The viscous stress tensor σ_{ij} is given by the constitutive relation $\sigma_{ij} = 2\mu S_{ij} + \frac{2}{3}(\lambda - \mu)S_{kk}\delta_{ij}$ where S_{ij} is the rate of strain tensor given by $S_{ij} = \frac{1}{2}(\partial u_i/\partial x_j + \partial u_j/\partial x_i)$.

The relevant nondimensional parameters are the Reynolds number Re and the Prandtl number Pr. It is important to point out that the energy equation (3) is expressed in terms of pressure because highlighting the character of pressure-velocity interactions is one of the main objectives of the present study. The full set of equations (1)–(3) for an ideal gas are solved in the numerical simulations and the linearized version is employed in the analysis.

We perform linear analysis for a general parallel streamline shear flow in which the flow of specific interest is a planar mixing layer. The inflectional instability of a mixing layer is inviscid in character and the only effect of viscosity is to damp disturbance amplitudes [18]. Thus the analysis is restricted to inviscid flow equations. Rather than eigenvalue analysis, we formulate an initial value problem [19] to identify the effect of perturbation obliqueness on the evolution of perturbation. The instantaneous field is decomposed into base and perturbation components:

$$q = \bar{q} + q', \quad q = q(\rho,u_1,u_2,u_3,p), \tag{4}$$

where $\bar{(.)}$ denotes a background or base quantity and $(.)'$ represents disturbance or perturbation. Applying the decomposition (4) to Eqs. (1)–(3) renders the evolution equation of the base quantities as follows:

$$\frac{\partial \bar{\rho}}{\partial t} + \bar{u}_j \frac{\partial \bar{\rho}}{\partial x_j} = \bar{\rho}\frac{\partial \bar{u}_j}{\partial x_j}, \tag{5}$$

$$\frac{\partial \bar{u}_j}{\partial t} + \bar{u}_k \frac{\partial \bar{u}_j}{\partial x_k} = -\frac{1}{\bar{\rho}}\frac{\partial \bar{p}}{\partial x_j}, \tag{6}$$

$$\frac{\partial \bar{p}}{\partial t} + \bar{u}_k \frac{\partial \bar{p}}{\partial x_k} = -\gamma \bar{p}\frac{\partial \bar{u}_k}{\partial x_k}. \tag{7}$$

A hyperbolic tangent profile is considered as the planar parallel shear base velocity:

$$\bar{u}_i = (U_1(x_2),0,0) = \left((\Delta U/2)\tanh\left(-x_2/2\delta_m^0\right),0,0\right), \tag{8}$$

where δ_m^0 is half of the initial mixing layer thickness and $(\Delta U/2)$ is the base velocity difference between the upper and lower streams of a mixing layer where $x_2 \to \pm\infty$. Here, x_1 is defined as the streamwise direction, x_2 is the normal direction, and x_3 is the spanwise direction. The initial pressure and density fields are taken to be spatially uniform [2,20]:

$$\bar{\rho}(x_1,x_2,x_3,0) \approx \bar{\rho}_0, \quad \bar{p}(x_1,x_2,x_3,0) \approx \bar{p}_0. \tag{9}$$

By subtracting the base flow from the instantaneous flow equations, the perturbation field evolution equations are obtained:

$$\frac{\partial \rho'}{\partial t} + U_1\frac{\partial \rho'}{\partial x_1} = -\frac{\partial(\bar{\rho}u_k')}{\partial x_k}, \tag{10}$$

$$\frac{\partial u_1'}{\partial t} + U_1\frac{\partial u_1'}{\partial x_1} = -u_2'\frac{\partial U_1}{\partial x_2} - \frac{1}{\bar{\rho}}\frac{\partial p'}{\partial x_1}, \tag{11}$$

$$\frac{\partial u_2'}{\partial t} + U_1\frac{\partial u_2'}{\partial x_1} = -\frac{1}{\bar{\rho}}\frac{\partial p'}{\partial x_2}, \tag{12}$$

$$\frac{\partial u_3'}{\partial t} + U_1\frac{\partial u_3'}{\partial x_1} = -\frac{1}{\bar{\rho}}\frac{\partial p'}{\partial x_3}, \tag{13}$$

$$\frac{\partial p'}{\partial t} + U_1\frac{\partial p'}{\partial x_1} = -\gamma\frac{\partial(\bar{p}u_k')}{\partial x_k}. \tag{14}$$

From Eqs. (11)–(13), the perturbation dilatation equation can be derived as

$$\frac{\partial}{\partial t}\left(\frac{\partial u_i'}{\partial x_i}\right) + U_1\frac{\partial}{\partial x_1}\left(\frac{\partial u_i'}{\partial x_i}\right) = -\frac{1}{\bar{\rho}}\frac{\partial^2 p'}{\partial x_i^2} - 2S\frac{\partial u_2'}{\partial x_1}, \tag{15}$$

where the background shear in the normal direction (S) is given by

$$S = \frac{\partial U_1}{\partial x_2}. \tag{16}$$

The right-hand side of Eq. (15) is obtained from the energy equation (3). To express the left-hand side of Eq. (15) exclusively in terms of pressure, the momentum equations (11)–(13) are differentiated with respect to t and the energy equation (14) is differentiated with respect to t and x_1:

$$\frac{\partial}{\partial t}\left(\frac{\partial u_i'}{\partial x_i}\right) = -\frac{1}{\gamma\bar{p}}\left(\frac{\partial^2 p'}{\partial t^2} + U_1\frac{\partial^2 p'}{\partial t\partial x_1}\right), \tag{17}$$

$$U_1\frac{\partial}{\partial x_1}\left(\frac{\partial u_i'}{\partial x_i}\right) = -\frac{U_1}{\gamma\bar{p}}\left(\frac{\partial^2 p'}{\partial t\partial x_1} + U_1\frac{\partial^2 p'}{\partial x_1^2}\right). \tag{18}$$

Substituting Eqs. (17) and (18) into Eq. (15), the evolution of the pressure perturbation can be expressed in a hyperbolic form of

$$\frac{\partial^2 p'}{\partial x_i^2} + 2\bar{\rho}S\frac{\partial u_2'}{\partial x_1} = \frac{1}{\bar{a}^2}\left(\frac{\partial^2 p'}{\partial t^2} + 2U_1\frac{\partial^2 p'}{\partial t\partial x_1} + U_1^2\frac{\partial^2 p'}{\partial x_1^2}\right), \tag{19}$$

where $\bar{a} = \sqrt{\gamma\bar{p}/\bar{\rho}}$ is the speed of sound in the base or background flow. Equation (19) is the evolution of the pressure perturbation in a general planar shear flow. In the incompressible limit $\bar{a} \to \infty$, reducing Eq. (19) to the familiar Poisson equation:

$$\nabla^2 p' \equiv \frac{\partial^2 p'}{\partial x_i^2} = -2S\bar{\rho}\frac{\partial u_2'}{\partial x_1}. \tag{20}$$

In this case, pressure has no thermodynamic significance and is merely a Lagrange multiplier imposing the incompressibility condition.

To facilitate further analysis, we apply the Howarth–Dorodnitsyn transformation [21]. The flow evolution is described in a coordinate moving with the background convective velocity:

$$X_1 = x_1 - \int_0^t U_1(x_2)\, d\xi, \quad X_2 = x_2, \quad X_3 = x_3, \quad t = t. \tag{21}$$

The perturbation equations (10)–(14) can be rewritten in the new coordinate frame as follows:

$$\frac{\partial \rho'}{\partial t} = -\bar{\rho}\left[\frac{\partial u_1'}{\partial X_1} + \frac{\partial u_2'}{\partial X_2} - \frac{\partial u_2'}{\partial X_1}S^* + \frac{\partial u_3'}{\partial X_3}\right], \tag{22}$$

$$\frac{\partial u_1'}{\partial t} = -\frac{1}{\bar{\rho}}\frac{\partial p'}{\partial X_1} - u_2'S, \tag{23}$$

$$\frac{\partial u_2'}{\partial t} = -\frac{1}{\bar{\rho}}\frac{\partial p'}{\partial X_2} + \frac{1}{\bar{\rho}}\frac{\partial p'}{\partial X_1}S^*, \quad (24)$$

$$\frac{\partial u_3'}{\partial t} = -\frac{1}{\bar{\rho}}\frac{\partial p'}{\partial X_3}, \quad (25)$$

$$\frac{\partial p'}{\partial t} = -\gamma\bar{p}\left[\frac{\partial u_1'}{\partial X_1} + \frac{\partial u_2'}{\partial X_2} - \frac{\partial u_2'}{\partial X_1}S^* + \frac{\partial u_3'}{\partial X_3}\right], \quad (26)$$

where

$$S^* = \int_0^t S(X_2)d\xi. \quad (27)$$

Starting from Eq. (19), the pressure equation in the new coordinates can be written as

$$\frac{1}{\bar{a}^2}\frac{\partial^2 p'}{\partial t^2} - \frac{\partial^2 p'}{\partial X_i^2} = -2\bar{\rho}S\frac{\partial u_2'}{\partial X_1}. \quad (28)$$

A. Initial value analysis

Initial value analysis entails the examination of the temporal development of small perturbations [22] imposed on the background velocity field. It is most convenient to consider simple Fourier perturbation modes [23,24].

Given the flow field homogeneity in the streamwise X_1 and spanwise X_3 directions, we seek to examine the evolution of disturbance modes of different degrees of obliqueness represented by

$$q' = \hat{q}(X_2,t)e^{i(\kappa_1 X_1 + \kappa_3 X_3)}, \quad (29)$$

where $i = \sqrt{-1}$ is the unit imaginary number, and $(\hat{\cdot})$ represents the Fourier amplitude of a perturbation mode. The wave number of the perturbation mode is given by $\vec{\kappa} = \kappa_1\vec{\mathbf{e}}_1 + \kappa_3\vec{\mathbf{e}}_3$, and κ_1 and κ_3 are the wave-number components in the streamwise and spanwise directions. The relative sizes of κ_1 and κ_3 determine the degree of disturbance obliqueness.

Considering the perturbation array of $q' = (\rho', u_i', p')$ and inserting the proposed ansatz of Eq. (29), the evolution equations of the Fourier amplitude of the perturbation field equations can be obtained from Eqs. (10)–(14):

$$\frac{\partial\hat{\rho}}{\partial t} = -\bar{\rho}\left[i\kappa_1\hat{u}_1 + \frac{\partial\hat{u}_2}{\partial X_2} - i\kappa_1\hat{u}_2 S^* + i\kappa_3\hat{u}_3\right], \quad (30)$$

$$\frac{\partial\hat{u}_1}{\partial t} = -\frac{i}{\bar{\rho}}\kappa_1\hat{p} - \hat{u}_2 S, \quad (31)$$

$$\frac{\partial\hat{u}_2}{\partial t} = -\frac{1}{\bar{\rho}}\frac{\partial\hat{p}}{\partial X_2} - \frac{i}{\bar{\rho}}\kappa_1\hat{p}S^*, \quad (32)$$

$$\frac{\partial\hat{u}_3}{\partial t} = -i\frac{\kappa_3}{\bar{\rho}}\hat{p}, \quad (33)$$

$$\frac{\partial\hat{p}}{\partial t} = -\gamma\bar{p}\left[i\kappa_1\hat{u}_1 + \frac{\partial\hat{u}_2}{\partial X_2} - i\kappa_1\hat{u}_2 S^* + i\kappa_3\hat{u}_3\right]. \quad (34)$$

It is evident from the above equations that the production rate perturbation kinetic energy is proportional to $\hat{u}_2 S$. Perturbation vorticity equation (not given here) also shows that $\hat{u}_2$ is critical in the generation of vorticity at all speed regimes. It is seen that $\hat{u}_2$ evolution hinges on that of perturbation pressure $\hat{p}$. Hence, the pressure-velocity ($\hat{p}$-$\hat{u}_2$) interaction holds the key to perturbation growth in all speed regimes [14]. Thus, this work proceed to examine how this interaction is influenced by compressibility and obliqueness.

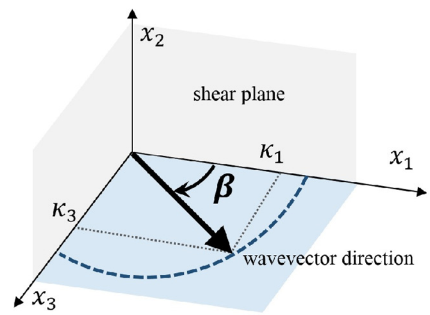

FIG. 1. A typical perturbation wave vector of obliqueness angle β. Here x_1, x_2, and x_3 are the streamwise, normal, and spanwise directions.

B. Pressure-velocity perturbation

To examine the obliqueness effect manifesting via the change in character of pressure, we return to the hyperbolic equation (19). Using Eqs. (31)–(34), we can obtain the evolution equation of the pressure amplitude:

$$\frac{1}{\bar{a}^2}\frac{\partial^2\hat{p}}{\partial t^2} = \frac{\partial^2\hat{p}}{\partial X_2^2} - \left(\kappa_1^2 + \kappa_3^2\right)\hat{p} + 2i\kappa_1\bar{\rho}\hat{u}_2 S + \left(i\kappa_1\frac{\partial S^*}{\partial X_2} + \kappa_1^2 S^{*2}\right)\hat{p}. \quad (35)$$

Equation (35) describes the evolution of pressure perturbation amplitude in an inhomogeneous form of wave equation where the first two terms of the right-hand side are the outcome of Laplace operator on $\hat{p}$ in the Fourier space and the remaining terms correspond to the source term.

To nondimensionalize Eq. (35), we introduce dimensionless time with shear as $t^* = \mathrm{St}$ and space with the wave-number magnitude as $x_i^* = \kappa x_i$. Equation (35) in the nondimensionalizing temporal and spatial coordinates can be rewritten as

$$\frac{S^2}{\bar{a}^2\kappa^2}\frac{\partial^2\hat{p}}{\partial t^{*2}} = \frac{\partial^2\hat{p}}{\partial x_2^{*}} - \hat{p} + 2i\left(\frac{\kappa_1}{\kappa}\right)\frac{\bar{\rho}}{\kappa}\hat{u}_2 S + \left[i\left(\frac{\kappa_1}{\kappa}\right)\frac{\partial S^*}{\partial x_2^*} + \left(\frac{\kappa_1}{\kappa}\right)^2 S^{*2}\right]\hat{p}. \quad (36)$$

To identify the role of perturbation orientation in the evolution pressure in a compressible mixing layer, we recognize the *obliqueness angle* β as the appropriate measure:

$$\beta \equiv \cos^{-1}\left(\frac{\kappa_1}{\kappa}\right), \quad (37)$$

where κ_1 is the *initial* value of the streamwise component of the wave vector and $\kappa = |\vec{\kappa}| = (\kappa_1^2 + \kappa_3^2)^{1/2}$ is the *initial* value of the wave-number magnitude. A typical oblique wave mode with its components on the shear plane are depicted in Fig. 1. Next, we identify the *gradient Mach number* M_g as the appropriate parameter to locally characterize the effect of compressibility on shear layer stability:

$$M_g \equiv \frac{Sl}{\bar{a}} = \frac{S}{\bar{a}\kappa}, \quad (38)$$

where l can be any relevant length scale of the flow that we associate it with $1/\kappa$ of a wave-mode perturbation. The other widely used Mach number in the compressible mixing layers studies is the *convective Mach number* M_c which is defined as $M_c \equiv \Delta U/2\bar{a}$. M_c is a global measure of the mixing layer compressibility, while M_g is a local measure of the effect of compressibility on the perturbation of wave number κ. The wave-like nature of pressure (36) can be written in a form wherein the effects of Mach number and obliqueness can be easily identified:

$$M_g^2\frac{\partial^2\hat{p}}{\partial t^{*2}} = \frac{\partial^2\hat{p}}{\partial x_2^*} - \hat{p} + 2i\frac{\bar{\rho}}{\kappa}\hat{u}_2 S\cos\beta + \left[i\frac{\partial S^*}{\partial x_2^*}\cos\beta + S^{*2}\cos^2\beta\right]\hat{p}. \tag{39}$$

Next, we nondimensionalize the velocity amplitude as $\hat{u}_i^* = \hat{u}_i/\bar{a}$ and the pressure amplitude as $\hat{p}^* = \hat{p}/\bar{p}^0$, where $\bar{p}^0$ is the initial background pressure. $\hat{u}_i^*$ can be interpreted as the *perturbation Mach number*. Hence, the final nondimensional form of Eq. (39) can be rewritten as

$$M_g^2\frac{\partial^2\hat{p}^*}{\partial t^{*2}} = \frac{\partial^2\hat{p}^*}{\partial x_2^*} - \hat{p}^* + 2i\gamma\hat{u}_2^* M_g\cos\beta + \left[i\frac{\partial S^*}{\partial x_2^*}\cos\beta + S^{*2}\cos^2\beta\right]\hat{p}^*. \tag{40}$$

Similarly, the velocity perturbation evolution can be described by an inhomogeneous wave equation. Differentiating Eq. (32) twice with respect to time yields

$$M_g^2\frac{\partial^2\hat{u}_2^*}{\partial t^{*2}} = \frac{\partial^2\hat{u}_2^*}{\partial x_2^{*2}} - i\frac{\hat{p}^*}{\gamma}M_g\cos\beta - \left[(\hat{u}_1^* - \hat{u}_2^* S^*)\cos^2\beta + \left(\hat{u}_3^*\sin\beta + i\frac{\partial\hat{u}_2^*}{\partial x_2^*}\right)\cos\beta\right]S^*. \tag{41}$$

Equations (40) and (41) clearly identify and isolate the effect of Mach number, perturbation wave number, and obliqueness on the evolution of small disturbances in general planar compressible shear flows. We now utilize the linearized equations to examine the influence of obliqueness on perturbation evolution and low and high speeds.

1. Pressure-velocity behavior at extreme β

Streamwise perturbations ($\beta = 0$) at low M_g. In the incompressible limit, the evolution of streamwise perturbations ($\beta = 0$) leads to the familiar KHI behavior. It has been demonstrated that p' and u_2' experience a positive feedback interaction [14]. As a result, the p' and u_2' evolution are nearly monotonic. The positive feedback causes an increasingly rapid overturning motion of the fluid in the interface region leading to mixing and instability growth.

Streamwise perturbations ($\beta = 0$) at large M_g. At compressible Mach numbers, the pressure-amplitude (40) and normal-velocity amplitude (41) equations for streamwise perturbations take the form of inhomogeneous wave equations:

$$M_g^2\frac{\partial^2\hat{p}^*}{\partial t^{*2}} - \frac{\partial^2\hat{p}^*}{\partial x_2^*} = \left(1 + S^{*2} + i\frac{\partial S^*}{\partial x_2^*}\right)\hat{p}^* + 2i\gamma M_g\hat{u}_2^*, \tag{42}$$

$$M_g^2\frac{\partial^2\hat{u}_2^*}{\partial t^{*2}} - \frac{\partial^2\hat{u}_2^*}{\partial x_2^{*2}} = -i\frac{\hat{p}^*}{\gamma} - \hat{u}_1^* S^* + \left(\hat{u}_2^* S^* - i\frac{\partial\hat{u}_2^*}{\partial x_2^*}\right)S^*. \tag{43}$$

This planar or zero obliqueness-angle perturbation has been investigated in detail by Karimi and Girimaji [14]. With increasing Mach number, the source term becomes weaker and the perturbations behave progressively like travelling waves. Closer inspection reveals that the source terms in the $\hat{p}$ and $\hat{u}_2$ equations (42) and (43) are out of phase. The resulting interactions between pressure p' and velocity u_2' represent negative, rather than positive, feedback. This leads to suppression of u_2' growth by compressibility effects and, more importantly, there is no overturning motion in the inflection-point region. In essence, the interface region experiences shaking, rather than stirring, motion. Such interface motion prohibits mixing and inhibits the growth of disturbance.

Spanwise perturbations ($\beta = \pi/2$) at arbitrary M_g. For this case, since $\cos\beta = 0$, the pressure and normal velocity equations (40) and (41) reduce to

$$M_g^2\frac{\partial^2\hat{p}^*}{\partial t^{*2}} = \frac{\partial^2\hat{p}^*}{\partial x_2^*} - \hat{p}^*, \quad M_g^2\frac{\partial^2\hat{u}_2^*}{\partial t^{*2}} = \frac{\partial^2\hat{u}_2^*}{\partial x_2^{*2}}. \tag{44}$$

This implies that $\hat{p}$ and $\hat{u}_2$ fields are decoupled and each one is governed by a simple wave equation. Because $\kappa_1 = 0$, $\hat{p}$ and $\hat{u}_1$ fields are also decoupled. For spanwise perturbations, the thermodynamic and flow fields evolve independently. Thus, the perturbation velocity field will evolve nearly independent of Mach number. This is similar to the *pressure-released limit* of flow evolution described by Simone *et al.* [12]. In incompressible mixing layers, Arratia *et al.* identify this as the lift-up instability (LUI) [25]. The pressure-released lift-up mechanism was first recognized in the context of boundary layers [26,27]. Our analysis clearly indicates that this lift-up mechanism is also important in compressible mixing layers as the evolution of spanwise perturbations is completely impervious to Mach number.

2. Behavior of oblique perturbations at $0 < \beta < \pi/2$

Having established flow perturbation behavior at extreme obliqueness angles in both high and low speeds, we next examine the behavior at intermediate angles. First we establish the effect of obliqueness in incompressible mixing layers and then proceed to examine the compressibility effects as a function of obliqueness.

Incompressible mixing layer. At the incompressible limit, pressure and normal velocity perturbation equations can be written as

$$\frac{\partial^2\hat{p}^*}{\partial x_2^*} - \hat{p}^* = -\left[i\frac{\partial S^*}{\partial x_2^*}\cos\beta + S^{*2}\cos^2\beta\right]\hat{p}^*, \tag{45}$$

$$\frac{\partial^2\hat{u}_2^*}{\partial x_2^{*2}} = \left[(\hat{u}_1^* - \hat{u}_2^* S^*)\cos^2\beta + \left(\hat{u}_3^*\sin\beta + i\frac{\partial\hat{u}_2^*}{\partial x_2^*}\right)\cos\beta\right]S^*. \tag{46}$$

First we identify two distinct contributions to the source term in Poisson pressure equation, the right-hand-side of Eq. (45). The shear gradient term represents the inhomogeneous shear effect and the second term indicates the homogeneous shear contribution. Both source terms diminish with increasing obliqueness angle. Thus, the magnitude of pressure fluctuations decrease with increasing obliqueness. Indeed, in the limit of spanwise fluctuations, the source term vanishes, indicating that there are no pressure fluctuations. The effect of obliqueness angle of u_2' is less evident. Due to the fact that u_2' evolution is exclusively by pressure, it can be surmised that diminishing pressure results in u_2' reduction with increasing obliqueness. At the spanwise limit, as previously established, there will be no growth in u_2' field. In the next sections, we use direct numerical simulations to establish the influence of obliqueness in incompressible mixing layers.

Compressible mixing layer. For arbitrary perturbation obliqueness $\beta \in (0,\pi/2)$, the pressure-velocity interaction is described by equations (40) and (41). In compressible flows, both shear and acoustic timescales influence the flow dynamics [28]. Therefore, temporal evolution of the perturbation via the pressure-velocity interaction can be more conveniently described with a geometric average of shear and acoustic times. Following homogeneous shear analysis of Kumar *et al.* [28], we also recognize that the effective shear experienced by an oblique perturbation is different from that of a streamwise or planar perturbation. We define effective shear S_e and new nondimensional time (τ) as follows:

$$S_e = S\cos\beta, \quad \tau = t\sqrt{\kappa\bar{a}S_e} = S_e t\sqrt{\cos\beta/M_g^e}, \tag{47}$$

where the *effective gradient Mach number* M_g^e is defined as

$$M_g^e = S_e/(\bar{a}\kappa) = M_g\cos\beta. \tag{48}$$

In a new normalized time τ, the pressure and normal velocity equations (40) and (41) can be expressed as

$$M_g^e\frac{\partial^2\hat{p}^*}{\partial\tau^2} = \frac{\partial^2\hat{p}^*}{\partial x_2^{*2}} - \hat{p}^* + \left[i\frac{\partial S_e^*}{\partial x_2^*} + S_e^{*2}\right]\hat{p}^* + 2i\gamma\hat{u}_2^* M_g^e, \tag{49}$$

$$M_g^e\frac{\partial^2\hat{u}_2^*}{\partial\tau^2} = \frac{\partial^2\hat{u}_2^*}{\partial x_2^{*2}} - i\frac{\hat{p}^*}{\gamma}M_g^e\left[\hat{u}_1^* S_e^*\cos\beta - \hat{u}_2^* S_e^{*2} + \left(\hat{u}_3^*\sin\beta + i\frac{\partial\hat{u}_2^*}{\partial x_2^*}\right)S_e^*\right]. \tag{50}$$

It is immediately evident that the oblique perturbation pressure equation (49) expressed in terms of equivalent shear and gradient Mach number is identical to that of the streamwise equation (42). The u_2' equations (50) and (43) are similar but not identical. Nevertheless, it is evident that the effective Mach number experienced by a perturbation diminishes as β increases from 0 to $\pi/2$. It is reasonable to conclude that the smaller the effective Mach number experienced by a perturbation, the lesser will be the influence of compressibility.

Inferences from linear analysis. In a high-Mach-number mixing layer, we now summarize the extent to which compressibility modifies the perturbation evolution (with respect to the incompressible baseline) as a function of obliqueness angle β. (i) Streamwise modes ($\beta = 0$) experience the largest effective Mach number and hence are most affected by compressibility. (ii) The influence of compressibility diminishes with increasing β as the effective Mach number decreases monotonically. (iii) There exists an obliqueness angle at which the effective Mach number is unity: $\beta_c = \cos^{-1}(\bar{a}\kappa/S)$. The critical angle β_c delineates subsonic and supersonic modes. (iv) At higher degrees of obliqueness ($\beta > \beta_c$), p'-u_2' interactions can be expected to be more similar to that of the incompressible case. Hence, the compressibility influence is likely to be small. (v) Spanwise modes ($\beta = \pi/2$) clearly evolve independent of Mach number as pressure and velocity fields are decoupled. The influence of obliqueness on suppression of energy growth and the existence of the critical obliqueness angle on the κ_1-κ_3 plane are depicted in Fig. 2. In the following sections, results from numerical simulations will be employed to examine the findings of linear analysis.

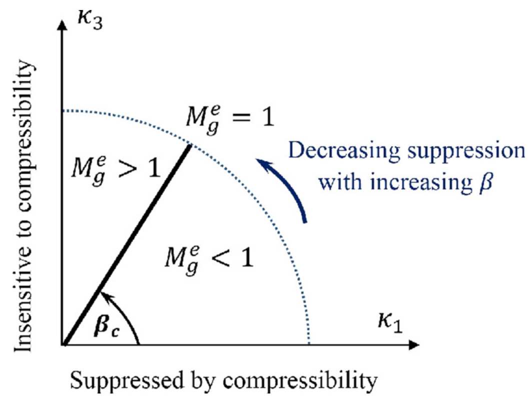

FIG. 2. Classification of oblique modes on the κ_1-κ_3 plane. β_c is the critical obliqueness angle where $M_g^e = 1$.

III. NUMERICAL APPROACH

The direct numerical simulation of small perturbation evolution in a compressible mixing layer is performed using the gas-kinetic method (GKM) [29]. This approach employs a hybrid kinetic scheme to effectively solve the full transport equations with all nonlinear and viscous physics completely intact. The GKM has gained popularity over the last decade, particularly in the context of compressible flow simulations as thermodynamic nonequilibrium effects can be handled with relative ease. The GKM scheme has been well validated for linear and nonlinear processes in high-speed shear flows [14,30,31].

Initial conditions. Due to the nature of the flow instability under consideration, it is reasonable to consider perturbations that are periodic in streamwise (x_1) and spanwise (x_3) directions. The perturbation velocity component responsible for instability is the normal (u_2) component. Therefore, only normal velocity perturbations are considered. Nonzero initial velocities in the other two directions do not modify the stability characteristics of the perturbations. The initial turbulence intensity can be set by adjusting the amplitude of the initial perturbation, u_2^0. To examine the effect of obliqueness, we identify three main types of perturbation modes: streamwise, spanwise, and oblique modes. This classification depends

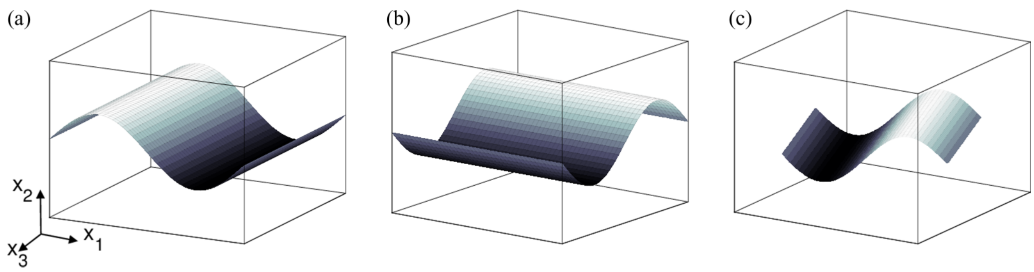

FIG. 3. Classification of perturbation modes based on their initial obliqueness angles β: (a) streamwise ($\beta = 0$), (b) spanwise ($\beta = \pi/2$), and (c) oblique ($0 < \beta < \pi/2$).

upon the direction of the modal wave vector. Figure 3 shows the schematic of the three different classes of initial condition perturbation fields used in the current DNS. The most general mode is an oblique mode. Oblique modes initially reside on the x_1-x_3 plane ($0 < \beta < \pi/2$). They combine characteristics of both spanwise and streamwise modes:

$$(u_1',u_2',u_3') = \left(0,u_2^0\sin(\kappa_1 x_1 + \kappa_3 x_3 + \phi),0\right), \qquad (51)$$

where $\boldsymbol{\kappa}(0)$ is the initial wave vector and $\hat{u_j}$ is the corresponding Fourier coefficient. The phase angle ϕ represents an arbitrary phase shift. Streamwise wave number (κ_1) and spanwise wave numbers (κ_3) set the value of the obliqueness angle of the perturbation mode. Since streamwise modes are initially aligned along the streamwise direction ($\beta = 0$), then $\kappa_3 = 0$ in Eq. (51). For spanwise modes that are are initially aligned normal to the shear plane ($\beta = \pi/2$), $\kappa_1 = 0$ in Eq. (51). The initial base velocity field has the form of Eq. (8).

Boundary conditions. In both the streamwise and spanwise directions periodic boundary conditions are used. The fluctuating field is taken to be periodic in normal direction. Following Thompson (1987), the nonreflective boundary condition is used in the normal direction for mean flow.

Simulation parameters. For all simulations presented here, $\hat{u}_2^0$ is set to $0.05\Delta U$ and $\phi = 0$ in Eq. (51). The initial density ratio between two streams is specified to unity. The initial background pressure is set to a uniform value. The initial temperature for all the cases is $T_0 = 300$. The initial momentum thickness Reynolds number is fixed to $\mathrm{Re}^0_{\delta_m} = 400$ for all cases at different initial convective Mach numbers. The Prandtl number is set to $\mathrm{Pr} = 0.7$. In the current simulations, air is used as the working fluid, thus, the gas constant is $R = 287\ \mathrm{J\,kg^{-1}\,K^{-1}}$ and the specific-heat ratio is $\gamma = 1.4$.

Having carefully verified and validated the numerical scheme and also performing exhaustive time-step and grid-size sensitivity studies [32,33], we now proceed with new simulations to highlight obliqueness effects on the small perturbation evolution in compressible mixing layers.

IV. SIMULATIONS, RESULTS, AND INFERENCES

Simulations are performed to assess the effect of obliqueness on instability in low- and high-Mach-number mixing layers. The findings are explained by using the results from the linear analysis. Each simulation is performed with single initial perturbation of a specific degree of obliqueness and its evolution is examined. The extent of perturbation evolution is characterized in terms of mixing metrics. The mixing metrics employed to assess instability evolution in a compressible mixing layer are (a) momentum thickness δ_m, (b) vorticity thickness δ_ω, (c) the perturbation kinetic energy, (d) the normal component of the perturbation kinetic energy, $R_{22} = \overline{u_2'u_2'}$. The definition of each mixing indicator and a brief discussion are presented in Appendix. All quantities are nondimensionalized with their initial value except the R_{22} which is normalized by the initial kinetic energy k_0. The temporal evolution of perturbations is examined in the *shear time*, which is the time normalized by the maximum initial shear rate: $t_s = (\Delta U/\delta_m^0)t$.

A. Quasi-incompressible case

We first establish the behavior of perturbations at different obliqueness angles in incompressible flows. By using the incompressible behavior at different obliqueness angles as the benchmark, we will then assess the compressibility effect at different perturbation orientations. The parameters of various simulations are given in Table I, where the cases are labeled according to their initial convective Mach number and obliqueness angles in degrees; e.g., case M7B30 is of $M_c = 0.7$ and $\beta = \pi/6$.

The evolution of various mixing metrics and energy components for the low-Mach-number case of $M_c = 0.3$ are shown in Fig. 4. It is important to recall that streamwise ($\beta = 0$) perturbations exhibit the well-known Kelvin–Helmholtz instability (KHI) and spanwise ($\beta = \pi/2$) perturbations display

TABLE I. Simulation parameters.

Case	M_c	β	κ	δ_m^0	$N_{x_1} \times N_{x_2} \times N_{x_3}$
M3B0	0.3	0	1	0.25	$256 \times 1024 \times 128$
M3B30	0.3	30	1	0.25	$256 \times 512 \times 128$
M3B60	0.3	60	1	0.25	$256 \times 512 \times 128$
M3B90	0.3	90	1	0.25	$256 \times 256 \times 128$
M7B0	0.7	0	1	0.25	$256 \times 1024 \times 128$
M7B30	0.7	30	1	0.25	$256 \times 512 \times 128$
M7B60	0.7	60	1	0.25	$256 \times 512 \times 128$
M7B90	0.7	90	1	0.25	$256 \times 256 \times 128$
M12B0	1.2	0	1	0.25	$256 \times 512 \times 128$
M12B30	1.2	30	1	0.25	$256 \times 512 \times 128$
M12B60	1.2	60	1	0.25	$256 \times 512 \times 128$
M12B90	1.2	90	1	0.25	$256 \times 256 \times 128$

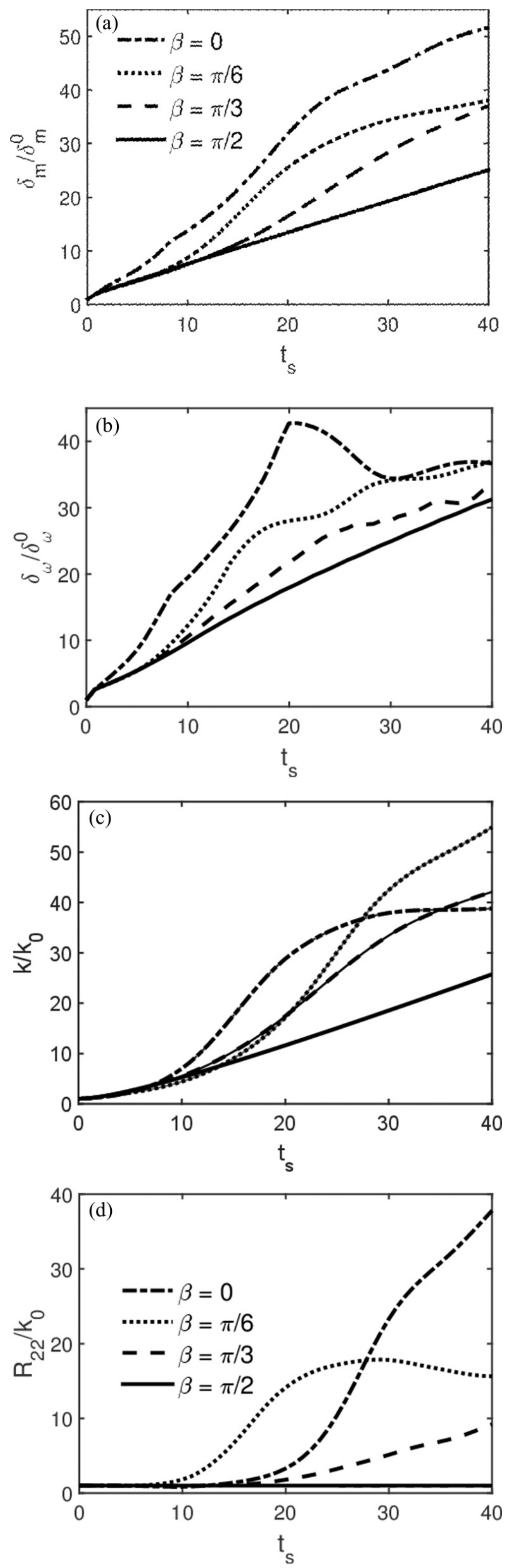

FIG. 4. Temporal evolution of (a) the normalized momentum thickness, (b) vorticity thickness, (c) the perturbation kinetic energy, and (d) $R_{22} = \overline{u_2' u_2'}/2$. Effect of obliqueness angle at $M_c = 0.3$.

lift-up instability (LUI). The nature of the instability also gradually changes with increasing obliqueness angle from KHI in the streamwise case toward LUI in the spanwise case. In the literature it is established that KHI is a modal instability whereas LUI is algebraic. This is evident from the early kinetic-energy growth. Figures 4(a) and 4(b) reveal that momentum and vorticity thickness growth slow down at early times (linear regime) with increasing obliqueness.

As indicated by the linear analysis, the normal fluctuations do not exhibit much change in the case of LUI ($\beta = \pi/2$), but grow rapidly with KHI ($\beta = 0$). This is depicted in Fig. 4(d). At intermediate obliqueness angles, the velocity evolution is not monotonic [see Figs. 4(c) and 4(d)] as the character of the instability gradually changes from KHI to LUI. The perturbation kinetic energy also exhibits a nonmonotonic transition from the slow growth of LUI to the rapid growth of KHI. Two useful inferences from the results exhibited in Fig. 4 are that (i) the KHI is better at mixing momentum and generating vorticity than LUI, and (ii) the growth of the perturbation kinetic energy is not directly proportional to growth of momentum or vorticity thickness. Having established the baseline incompressible behavior, we now investigate how compressibility modifies this behavior at different obliqueness angles.

B. Streamwise modes ($\beta = 0$)

The temporal evolution of streamwise perturbation (51) when $\kappa_3 = 0$ is now examined in detail [14]. To establish the role of the obliqueness angle, results from this case are shown in Fig. 5. The effect of Mach number is immediately evident. At low Mach number, vorticity thickness grows rapidly through the linear stage and saturates (at $t_s \approx 23$) within the shown time duration. At this time, the first roll-up occurs in the evolution of KHI.

The growth of each mixing metric is suppressed progressively with increasing Mach number. At higher Mach numbers, the growth is slow and all metrics are still in the initial regime of development in the time duration shown. Linear analysis indicates that change in character of pressure from a simple Lagrange multiplier in incompressible flow to a wave at high Mach numbers results in inhibition of u_2'. The simulation results clearly indicate reduction in normal velocity magnitude confirming the findings of linear analysis; see Fig. 5(d). This reduction in turn results in decreased kinetic-energy production, vorticity generation, and mixing. Clearly the effect of compressibility on streamwise fluctuations is very pronounced.

C. Spanwise modes ($\beta = \pi/2$)

The temporal evolution of the mixing indicators at different M_c for the spanwise modes (51) when $\kappa_1 = 0$ is shown in Fig. 6. Regardless of the initial convective Mach number, momentum and vorticity thickness shown in Figs. 6(a) and 6(b), respectively, grow at nearly the same rate under the influence of the lift-up instability. The same trend can be observed in the evolution of the normalized kinetic energy, as shown in Fig. 6(c). Most notably, u_2' remains at its initial value at all Mach numbers, as demonstrated in Fig. 6(d).

As anticipated from linear analysis, the growth of the spanwise perturbations is impervious to compressibility. All these findings are consistent with the principal findings of linear analysis (44): (i) u_2' does not grow due to the fact that

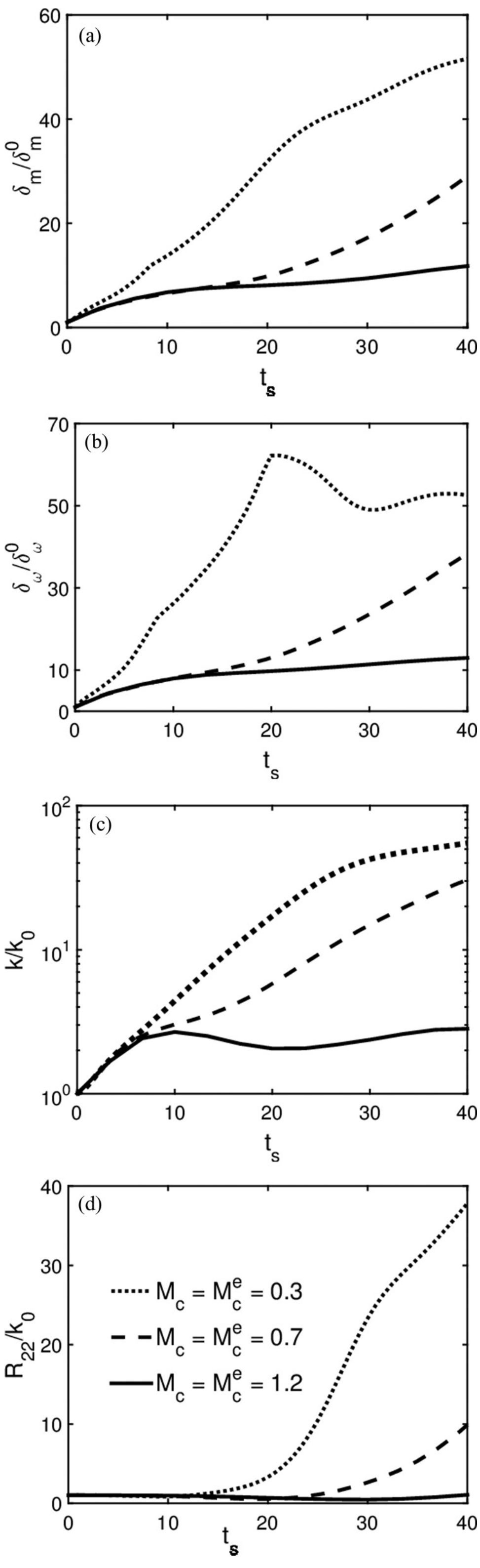

FIG. 5. Temporal evolution of (a) the normalized momentum thickness, (b) vorticity thickness, (c) the perturbation kinetic energy, and (d) $R_{22} = \overline{u_2'u_2'}/2$. Effect of convective Mach number at $\beta = 0$.

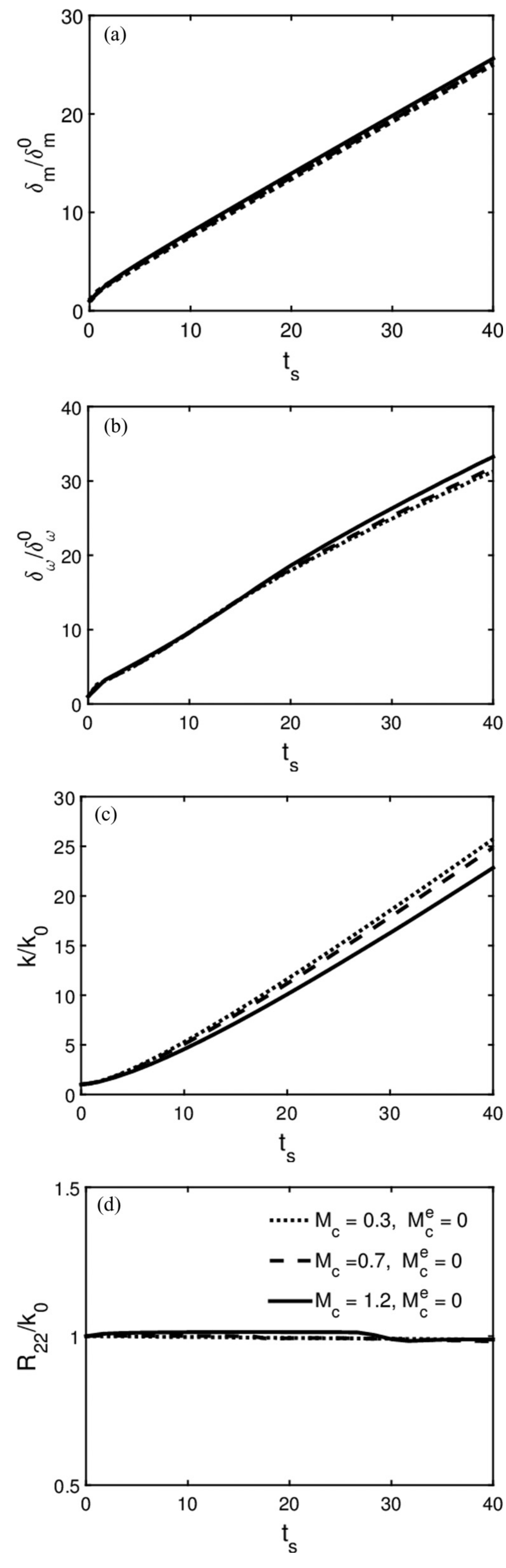

FIG. 6. Temporal evolution of (a) the normalized momentum thickness, (b) vorticity thickness, (c) the perturbation kinetic energy, and (d) $R_{22} = \overline{u_2'u_2'}/2$. Effect of convective Mach number at $\beta = \pi/2$.

it is entirely decoupled from the pressure field, and (ii) this decoupling occurs at all Mach numbers and, therefore, the evolution of perturbation is independent of Mach number.

D. Oblique modes, $\beta \in (0,\pi/2)$

We now examine the perturbation evolution at intermediate obliqueness angles of $\pi/6$ and $\pi/3$. The initial velocity perturbation is of the form of Eq. (51) where the values of κ_1 and κ_3 are chosen to yield the required value of β. Clearly, these modes can be expected to display features of both KHI and LUI to varying degrees. The temporal evolution of the mixing indicators for two obliqueness angles of $\beta = \pi/3$ and $\beta = \pi/6$ are shown in Figs. 7 and 8, respectively. For a given obliqueness angle, we compare the evolution of various metrics at different Mach numbers. The larger the deviation from the incompressible behavior, the stronger is the compressibility effect.

It is immediately evident that $\beta = \pi/6$ case exhibits KHI-type behavior at lower Mach numbers. Close examination of the early evolution ($t_s < 10$) of momentum thickness and vorticity thickness at these two oblique angles of $\beta = 0$ and $\pi/6$ clearly indicates an important trend: the thickness growth rates at different Mach numbers get progressively closer to the baseline incompressible behavior with increasing obliqueness angle. Correspondingly, the evolution of kinetic energy and normal-velocity amplitude also exhibit increasingly similar behavior. Modes aligned closer with streamwise direction are clearly more suppressed by compressibility. The implication is that the suppressive influence of compressibility diminishes with with increasing obliqueness. Equally evident is the fact that the nature of early growth of the various metrics goes from exponential at low obliqueness angles to algebraic at higher angles. While KHI tendencies are suppressed by compressibility, the LUI-type behavior is reasonably unaffected.

In summation, (i) for a given M_c, perturbation suppression diminishes with increasing of β and, (ii) for a given β, perturbation suppression intensifies with increase of M_c. These findings are entirely consistent with linear analysis which stipulates decreasing effective Mach number with increasing obliqueness.

The results shown offer further interesting insights into early time behavior at different obliqueness angles. At each obliqueness angle, the various thicknesses and energy components display identical evolution at higher Mach numbers. It is demonstrated that, for high-Mach-number shear flows, perturbation evolution occurs in three stages demarcated on the basis of the timescale ratio of pressure and shear fields [28]. Initially, pressure field evolves slowly in comparison to shear timescale. With time, it is shown that the pressure timescale decreases monotonically. At intermediate times, pressure and shear timescales are comparable. Ultimately, the pressure timescale becomes smaller than that of shear. At early times, slowly evolving pressure field does not influence the perturbation growth. This time regime is called the "pressure-released" regime. During this period, the perturbation experiences a lift-up type growth which is independent of Mach number. This behavior is clearly seen in the early times of perturbation evolution at all obliqueness angles. Beyond this time, pressure effects manifest and the behavior at different Mach numbers begins to deviate.

Next we examine gradient Mach number equivalence (M_g^e) at different obliqueness angles. In homogeneous shear flows, it is established that perturbation evolution of different obliqueness angles and Mach numbers are identical in the linear regime provided that the equivalent Mach numbers are the same [28]. In a mixing layer such a demonstration is not possible because the shear is not uniform in the flow domain. For mixing layers we define equivalent convective Mach number:

$$M_c^e = M_c \cos\beta. \quad (52)$$

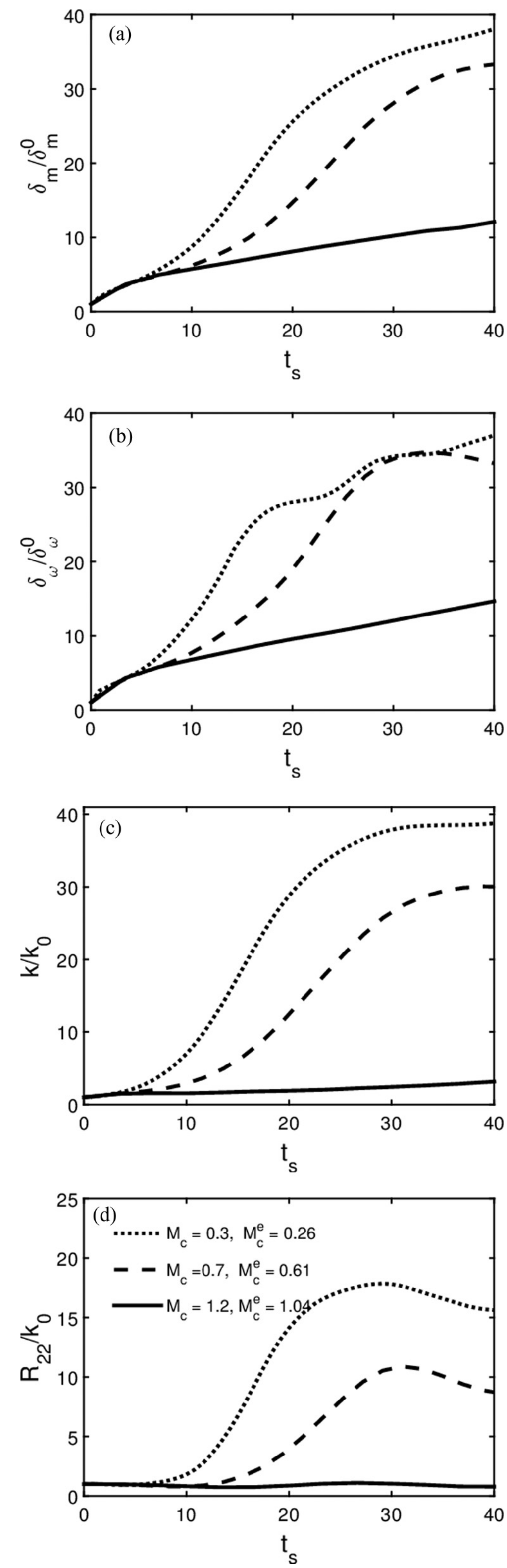

FIG. 7. Temporal evolution of (a) the normalized momentum thickness, (b) vorticity thickness, (c) the perturbation kinetic energy, and (d) $R_{22} = \overline{u_2' u_2'}/2$. Effect of convective Mach number at $\beta = \pi/6$.

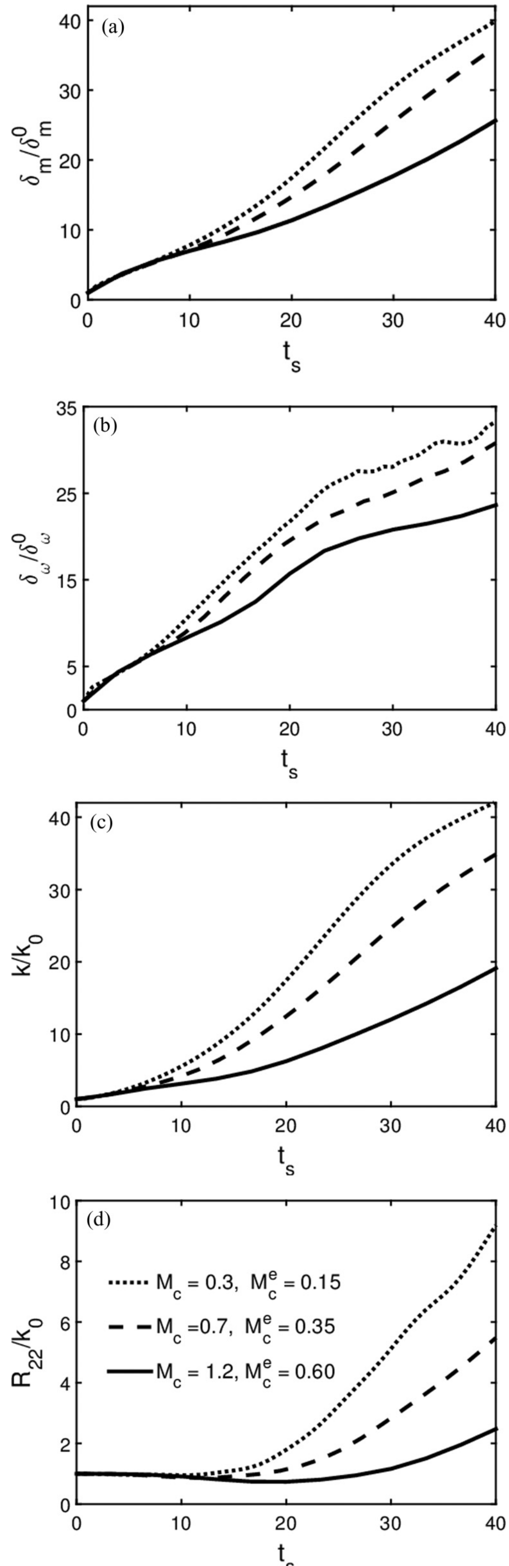

FIG. 8. The temporal evolution of (a) the normalized momentum thickness, (b) vorticity thickness, (c) the perturbation kinetic energy, and (d) $R_{22} = \overline{u_2' u_2'}/2$. Effect of convective Mach number at $\beta = \pi/3$.

While M_c^e does not lead to precise self-similarity, we investigate if qualitative similarities exist in the evolution of two perturbations at different obliqueness and Mach numbers, but the same M_c^e. Comparison of the dashed lines in Fig. 7 ($\beta = \pi/6$, $M_c = 0.7$, $M_c^e \approx 0.61$) with the solid lines in Fig. 8 ($\beta = \pi/3$, $M_c = 1.2$, $M_c^e \approx 0.6$) show nearly similar behavior at early times ($t_s < 10$).

It should be pointed out that simulations with perturbations of higher initial wave numbers were also performed. The results were similar to those presented here (with $\kappa = 1$), except viscous effects manifested sooner than in the lower-wave-number cases.

V. CONCLUSION

Compressibility has a profound effect on the stability of shear layers with inflection point. In this article, we examine the critical influence of perturbation orientation—with respect to the shear plane—that affects stability characteristics of high-speed planar shears layers with an inflection point. The effect of obliqueness is established by analyzing an initial value problem of the linearized perturbation equations. The inferences of the analysis are then validated by performing direct numerical simulations (DNS) of a compressible mixing layer with a single initial perturbation.

Linear analysis clearly shows that the stabilizing influence of compressibility diminishes with increasing obliqueness angle of the perturbation. Perturbations on the shear plane are stabilized by compressibility (increasing Mach number), whereas spanwise perturbations are exhibit the same degree and type (LUI) of instability at all Mach numbers. This outcome of linear analysis is confirmed by performing DNS of compressible mixing layer with a single perturbation mode. The findings from this work are expected to contribute toward improved insight into high-speed shear layer instability.

ACKNOWLEDGMENTS

This work was partially supported by the National Center for Hypersonic Laminar-Turbulent Transition Research at Texas A&M University.

APPENDIX: MIXING INDICATORS

Mixing layer growth can be characterized by the following metrics.

1. Momentum thickness (δ_m)

Momentum thickness, which is used as a measure of the spreading rate in mixing layers, is defined by

$$\delta_m(t) = \frac{1}{\bar{\rho}_0 \Delta U^2} \int_{-\infty}^{\infty} \bar{\rho}\left(\frac{1}{4}\Delta U^2 - u_1^2\right) dx_2, \quad \text{(A1)}$$

where ΔU is a velocity difference between two streams of mixing layer flows.

2. Vorticity thickness (δ_ω)

Vorticity thickness, as another measure of the spreading rate in mixing layers, is defined by

$$\delta_\omega(t) = \frac{\Delta U}{(\partial \bar{u}_1/\partial x_2)_{\max}}, \quad \text{(A2)}$$

where $(\partial \bar{u}_1/\partial x_2)_{\max}$ occurs at the inflection point of the mean velocity profile. Momentum thickness and vorticity thickness can be related to each other. The correlation between them depends on the initial values of the convective Mach number and the velocity ratio between two streams [13].

The vorticity thickness is found to be a more sensitive measure of shear-layer thickness than the momentum thickness [10].

3. Perturbation kinetic energy (*k*)

Besides using momentum thickness and vorticity thickness, the growth of instability in mixing layers can be examined by monitoring the temporal evolution of the perturbation kinetic energy k, which is defined by

$$k = \frac{1}{2}\overline{u_i'u_i'} = \frac{1}{\boldsymbol{V}}\int_V u_i'u_i'dx_i, \tag{A3}$$

where $\boldsymbol{V}$ is the total volume of the computational domain and over-line represents the volume-averaged of the quantity.

4. Normal Reynolds stress R_{22}

Due to the presence of the inhomogeneity in the x_2 direction in mixing layers, the evolution of the normal Reynolds stress

$$R_{22} = \tfrac{1}{2}\overline{u_2'u_2'} \tag{A4}$$

is also extremely valuable in examining the growth of instability.

[1] P. J. Schmid and D. S. Henningson, *Stability and Transition in Shear Flows* (Springer-Verlag, Berlin, Heidelberg, New York, 2001).
[2] S. Chandrasekhar, *Hydrodynamic and Hydromagnetic Stability* (Oxford Clarendon Press, London, 1961).
[3] A. Sen, Effect of compressibility on Kelvin–Helmholtz instability in a plasma, Phys. Fluids **7**, 1293 (1964).
[4] A. Miura, Kelvin–Helmholtz instability at the magnetospheric boundary: Dependence on the magnetosheath sonic Mach number, J. Geophys. Res. **97**, 10655 (1992).
[5] M. G. Gudkov and O. A. Troshichev, Kelvin–Helmholtz instability in a compressible plasma with a magnetic field and velocity shear, J. Atmos. Terr. Phys. **58**, 613 (1996).
[6] N. Chinzei, G. Masuya, T. Komuro, A. Murakami, and K. Kudou, Spreading of two-1stream supersonic turbulent mixing layers, Phys. Fluids **29**, 1345 (1986).
[7] D. Papamoschou and A. Roshko, The compressible turbulent shear layers: An experimental study, J. Fluid Mech. **9**, 453 (1988).
[8] G. S. Elliott and M. Samimy, Compressibility effects in free shear layers, Phys. Fluids **2**, 1231 (1990).
[9] A. J. Smits and J.-P. Dussauge, *Turbulent Shear Layers in Supersonic Flows*, 2nd ed. (Springer, Princeton University, 2006).
[10] N. D. Sandham and W. C. Reynolds, Three-dimensional simulations of large eddies in the compressible mixing layer, J. Fluid Mech. **224**, 133 (1991).
[11] A. W. Vreman, N. D. Sandham, and K. H. Luo, Compressible mixing layer growth rate and turbulence characteristics, J. Fluid Mech. **320**, 235 (1996).
[12] A. Simone, G. N. Coleman, and C. Cambon, The effect of compressibility on turbulent shear flow: A rapid distortion theory and direct-numerical-simulation study, J. Fluid Mech. **330**, 307 (1997).
[13] C. Pantano and S. Sarkar, A study of compressibility effects in the high-speed turbulent shear layer using direct simulation, J. Fluid Mech. **451**, 329 (2002).
[14] M. Karimi and S. S. Girimaji, Suppression mechanism of Kelvin–Helmholtz instability in compressible fluid flows, Phys. Rev. E **93**, 041102 (2016).
[15] M. Lessen, J. A. Fox, and H. M. Zien, On the inviscid instability of laminar mixing of two parallel streams of a compressible fluid, J. Fluid Mech. **23**, 355 (1965).
[16] T. L. Jackson and C. E. Grosch, Inviscid spatial stability of a compressible mixing layer, J. Fluid Mech. **208**, 609 (1989).
[17] N. D. Sandham, Y. Yao, L. Krishnan, and G. T. Roberts, The effect of Mach number on unstable disturbances in shock/boundary layer interactions, Phys. Fluids **19**, 054104 (2007).
[18] R. Betchov and A. Szewczyk, Stability of a shear layer between parallel streams, Phys. Fluids **6**, 1391 (1963).
[19] P. L. Pritchett, C. C. Wu, and J. M. Dawson, Interchange instabilities in a compressible plasma, Phys. Fluids **21**, 1543 (1978).
[20] P. G. Drazin and W. Reid, *Hydrodynamic Stability* (Cambridge University Press, New York, 1981).
[21] L. Howarth, Concerning the effect of compressibility on laminar boundary layers and their separation, Proc. R. Soc. London, Ser. A **194**, 16 (1948).
[22] R. Betchov and W. O. Criminale, *Stability of Parallel Flows*, 1st ed. (Academic Press, New York, 1967).
[23] B. J. Bayly, Three-Dimensional Instability of Elliptical Flow, Phys. Rev. Lett. **57**, 2160 (1986).
[24] M. J. Landman and P. G. Saffman, The three-dimensional instability of strained vortices in a viscous fluid, Phys. Fluids **30**, 2329 (1987).
[25] C. Arratia, C. P. Caulfield, and J.-M. Chomaz, Transient perturbation growth in time dependent mixing layers, J. Fluid Mech. **760**, 90 (2013).
[26] T. Ellingsen and E. Palm, Stability of linear flow, Phys. Fluids **18**, 487 (1975).
[27] M. T. Landahl, A note on an algebraic instability of inviscid parallel shear flows, J. Fluid Mech. **98**, 243 (1980).
[28] G. Kumar, R. L. Bertsch, and S. S. Girimaji, Stabilizing action of pressure in homogeneous compressible shear flows: Effect of Mach number and perturbation obliqueness, J. Fluid Mech. **760**, 540 (2014).
[29] K. Xu, A gas kinetic BGK scheme for the Navier–Stokes equations and its connection with artificial dissipation and Godunov method, J. Comput. Phys. **171**, 289 (2001).
[30] G. Kumar, S. S. Girimaji, and J. Kerimo, Weno-enhanced gas-kinetic scheme for direct simulations of compressible transition and turbulence, J. Comput. Phys. **234**, 499 (2012).
[31] Z. Xie and S. S. Girimaji, Instability of Poiseuille flow at extreme Mach numbers: Linear analysis and simulations, Phys. Rev. E **89**, 043001 (2014).
[32] M. Karimi, Ph.D. thesis, Texas A&M University, 2015 (unpublished).
[33] Z. Xie, M. Karimi, and S. S. Girimaji, Small perturbation evolution in compressible Poiseuille flow: pressure-velocity interactions and obliqueness effects, J. Fluid Mech. **814**, 249 (2017).